



Effects of cadmium ion concentration on the optical and photo-response properties of CdSe/PVP nanocomposites for white light sensing application

K. C. Handique¹ · P. K. Kalita¹

Received: 24 July 2020 / Accepted: 20 August 2020 / Published online: 31 August 2020
© Springer-Verlag GmbH Germany, part of Springer Nature 2020

Abstract

Cadmium selenide (CdSe) nanoparticles dispersed in the PVP matrix with varying concentrations of cadmium (Cd) ion complex have been synthesized through a low-cost chemical bath deposition technique to investigate the effects of cadmium ion concentration on its optical and photo-response characteristics. To confirm the formation of pure, stable, well dispersed, and highly crystalline spherical CdSe nanocomposites different characterization techniques such as X-ray diffraction, field emission scanning electron microscopy, high-resolution transmission electron microscopy, and Fourier transform infrared spectroscopy have been used. The optical band gaps and sizes of the nanocomposites are determined from the UV–Vis data while the surface-related emission properties of the CdSe nanocomposites are obtained from the PL data. The quantum confinement on the CdSe nanocomposites increases with the decrease of Cd ion concentration. I–V characteristics measurements have been done on the samples to investigate the photo-response properties of the samples. Various optical properties such as bandgap, near bandgap emission, and impurity emission are correlated with the photo-response properties of the samples. The photoresponse properties are found to become more suitable for application in white light photosensor with the increase of quantum confinement. Mechanisms related to the enhancement of photocurrent with respect to quantum confinement are also discussed in this paper.

Keywords CdSe nanoparticle · Cd ion concentration · Absorption · Photoluminescence · Photodetector

1 Introduction

Cadmium selenide nanoparticles have been attracting vast interest among the research community in recent years for its high demand in terms of optoelectronic applications [1–3]. It is a widely used semiconductor material which possesses a direct bandgap of 1.74 eV at room temperature and Bohr radius 5.6 nm [4]. The increased size to volume ratio and the quantum size effect is the key reason for which it can find enormous applications in various fields ranging from light-emitting diode to solar cells [5–9]. Many workers are trying to produce and study various properties of this type of II–VI semiconductors in cost-effective ways. Chemical bath deposition is a comparatively low-cost technique for

producing nanomaterials as it doesn't require highly sophisticated instruments. CdSe nanostructures have already been synthesized by many workers using various techniques such as precipitation, microwave deposition, sputtering, sonochemical, solvothermal etc. [10–13]. In the synthesis of nanostructures growth temperature, annealing temperature, the volumetric ratio of the precursor solutions play an important role in the properties of the materials to be synthesized. The size of the nanoparticle is again solely dependent on the growth temperature and the other above mentioned factors. To prevent the agglomeration or faster growth of the particles, capping agents are also commonly used which results in the mitigation of growth of the nanoparticles and stabilizes the smaller sized particles in a solution and thus improves various optoelectronic properties of the host material. The selection of a proper eco-friendly capping agent is sometimes a bit challenging because many of the commercially available capping agents are toxic to the environment. PVP (polyvinyl pyrrolidone) is a widely used capping agent because it contains some nontoxic eco-friendly functional groups

✉ K. C. Handique
kshirud.handique@rgu.ac.in

¹ Department of Physics, Rajiv Gandhi University, Itanagar, Arunachal Pradesh 791112, India

[14]. It is also expectable that the molar concentration of the various compositional complexes can play a crucial role in the reaction kinetics of CdSe nanostructures which is not reported yet to the best of our knowledge. Photoresponse characteristics of CdSe nanoparticle is also of considerable interest over the years from the application point of view in optoelectronic devices [15–19].

Keeping in view of the above aspects we have synthesized CdSe nanostructures using PVP as a capping agent with different molar concentrations of Cd ion complex. Emphasis has been given on the study of optical and photoresponse properties corresponding to its growth. The effects of the Cd ion concentration on the reaction kinetics and thus on the optical and photoresponse properties of the as-synthesized CdSe nanostructures are studied in this paper. Thus the modulated optical properties due to the varying Cd ion concentration is correlated with the photoresponse characteristics and exploited in the fabrication of white light photosensor.

2 Experimental

2.1 Materials used

All the chemicals and reagents used in the synthesis are purchased from Merck and used with no further purification. In our synthesis of PVP capped CdSe nanoparticles we have used cadmium acetate ($\text{Cd}(\text{CH}_3\text{COO})_2 \cdot 2\text{H}_2\text{O}$, purity 99%), black selenium powder (Se, purity 99.9%), ammonia solution (25%), sodium sulphite (Na_2SO_3), hydrazine hydrate ($\text{N}_2\text{H}_4 \cdot \text{H}_2\text{O}$, 24% solution in water) and polyvinyl pyrrolidone (PVP) ($\text{C}_2\text{H}_5\text{NO}$)_n. Double deionized water is used as the aqueous medium in all the synthesis.

2.2 Synthesis of CdSe/PVP nanocomposites

For the synthesis of CdSe nanoparticles initially, cadmium and selenium ion complexes are prepared separately. PVP is used as the capping agent for bringing the quantum

confinement on the samples. Cadmium ion complex is prepared by adding 13.3 gm (0.5 M) of cadmium acetate in 100 ml 3% PVP solution. Sodium selenosulphate is used as the selenium source prepared by dissolving black selenium powder (2.96 gm) and sodium sulphite (Na_2SO_3) (18.9 gm) in 100 ml 3% PVP solution. The mixture is stirred with a magnetic stirrer at temperature 95 °C for 5 h to get fresh sodium selenosulphate (Na_2SeSO_3) solution. A small amount of ammonia (3–4 drops) and 10 ml of hydrazine hydrate are added to the Cd ion complex and sodium selenosulphate solution respectively for faster growth of CdSe nanocrystals. Here the role of hydrazine hydrate is to provide alkalinity to the solution mixture and a homogeneous solution environment for the reaction by forming a complex with Cd^{2+} and to avoid the precipitation of CdSeO_3 [20–22]. Now the Cadmium ion complex and the sodium selenosulphate are mixed and stirred for 2 h until the formation of reddish-yellow colored CdSe crystals. This sample is coded as C0.5. Similarly other four samples viz. C 0.1, C0.01, C0.005 and C 0.001 are prepared by taking the molar concentration of cadmium acetate as 0.1 M, 0.01 M, 0.005 M and 0.001 M keeping the other parameters fixed. A schematic representation of the reaction mechanism involved during the formation of CdSe nanoparticles is shown in Fig. 1. The concentration of selenium ion in the form of sodium selenosulphate has been kept constant for all the remaining samples. Thus by taking the concentration of selenium ion fixed, we are varying the concentration of cadmium ions only. In the reaction, the CdSe nanoparticles dispersed in the PVP matrix are capped by the functional group of PVP, thus preventing the aggregation of nanoparticles. During the process PVP also plays an important role in enhancing the monodisperse property of CdSe nanoparticles. It also modifies the Oswald ripening kinetics of the reactions in such a way that the growth rate decreases with the size of the nanocomposites and effectively narrow the size distribution [23–25].

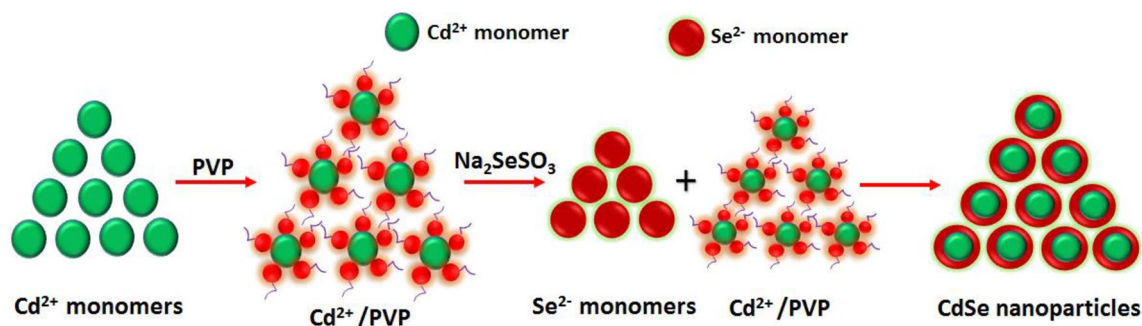
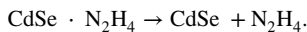
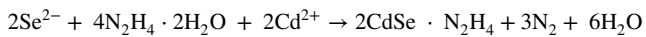
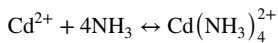
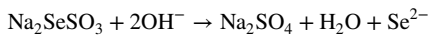
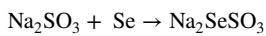


Fig. 1 Schematic diagram of reaction kinetics during the formation of CdSe nanoparticles

The reactions involved during the synthesis are shown below [20]



2.3 Fabrication of white light photosensor

The white light photosensor was fabricated on a printing copper board (PCB) where a copper layer is coated on an insulating substrate. After proper masking of the electrodes on the substrate (PCB) the other portions of the substrate are etched out by dissolving it in a ferric chloride solution. The square size area between the electrodes for the deposition of the CdSe nanocomposite layer is taken as 0.25 cm^2 . After proper etching, the substrate is washed with acetone multiple times and dried in a hot air oven. Thus the electrodes are designed on the substrate and the synthesized sample solution of CdSe nanocomposite is drop casted on the proper area and allowed to dry in a hot air oven at a temperature 100°C . The electrical measurements (I–V response) at dark conditions are done with a Keithley source meter. A set up combined with a halogen light that emits white light in the visible region is used to illuminate the channel area of the photosensor. A schematic diagram of the as-fabricated CdSe nanoparticle-based photosensor is shown in Fig. 2. A Lutron lux meter (model:LX-101A) is used to determine the intensity of the incident light.

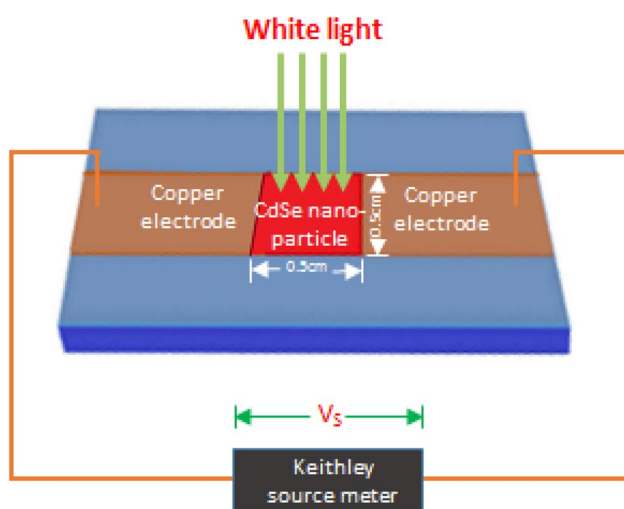


Fig. 2 Schematic diagram of CdSe nanoparticle based photodetector under white light illumination

2.4 Characterization

The synthesized nanoparticles are characterized by X-ray diffraction, UV–Vis, and photoluminescence (PL) spectroscopy. The XRD spectra have been taken using an ULTIMA IV X-Ray diffractometer with $\text{CuK}\alpha$ radiation of 0.1542 nm wavelength operated at 40 mA and 40 kV current and voltage respectively. Sample in powder form is used for taking the XRD diffractogram. For that, the impurities dissolved in the sample is washed out with methanol multiple times and the sample is centrifuged with a Remi high power centrifuge (model: PR-24) with 9000 rpm . Then the sample is dried in a hot air oven to make it powder form. The UV–Vis spectra is taken with the help of an Agilent technologies 60 Cary eclipse spectrometer with scanning range $300\text{--}800 \text{ nm}$. Double deionized water is used as the reference solvent prior to the measurement on CdSe sample. A Cary eclipse fluorescence spectrometer is used for the measurement of PL on the samples in the range $435\text{--}635 \text{ nm}$. The excitation wavelength is taken at 370 nm . Baseline corrections have been done for all the measurements. FESEM images are taken with the help of a Zeiss FESEM. The elemental composition of CdSe nanoparticles is determined with the help of the EDS setup attached to Zeiss FESEM. For high-resolution TEM *JEM 2100* electron microscope is used. The I–V measurements on the devices are done with a source meter (model: keithley-2450) both at dark and illumination with white light of intensity 1.8 mW/cm^2 . As we are using white light for illuminating the device sensing area we are taking the mean value of wavelength for the entire visible region for the ease of doing calculations. Two probe measurement configuration is used in the source meter with the voltage range from -5 to 5 V for the measurement of I–V response.

3 Results and discussion

3.1 X-ray diffraction analysis

The X-ray diffraction spectroscopy has been done on a particular sample C0.5 M synthesized by taking 0.5 M cadmium ion complex to determine the phase and structure of the prepared nanoparticles. A large peak broadening in the entire range of 2θ from 20° to 80° exhibits a promising nanocrystalline structure as shown in Fig. 3. Three clear diffraction peaks can be seen from the spectra which are later identified as (111), (220), and (311) planes with polycrystalline cubic zinc blende structure after comparing it with the standard JCPDS data (JCPDS card no-19-019) [26]. The lattice parameter of the as-prepared CdSe nanocrystal is calculated from the XRD data and it is found as 0.5988 nm using Eq. (1) that agrees well with the standard one. The

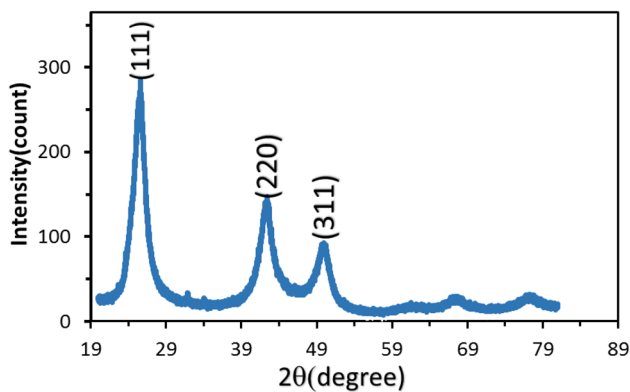


Fig. 3 X-Ray Diffraction Spectra of CdSe nanoparticles (C0.5 M)

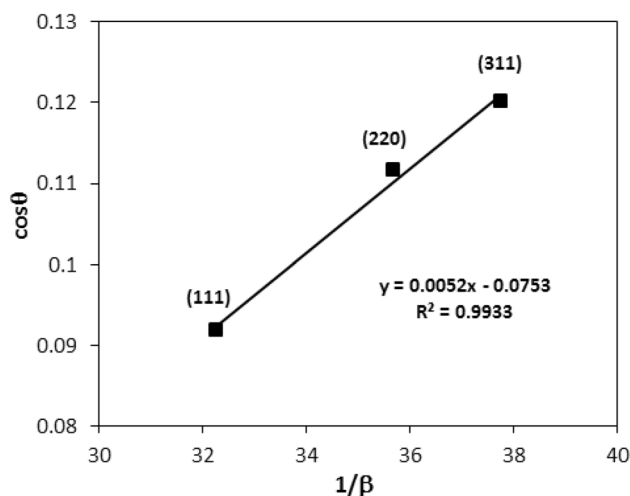


Fig. 4 Debye Scherer Plot for CdSe nanoparticles (C0.5 M)

well-known Scherer plot is used to determine the average crystallite size of the nanoparticles as shown in Eq. (2)

$$d_{hkl} = a / (h^2 + k^2 + l^2)^2, \tag{1}$$

$$D = K\lambda / \beta \cos \theta, \tag{2}$$

where D is the particle size and λ is the wavelength of the x-ray used, β is the FWHM of the Bragg peak and θ is the diffracting angle. The Scherer plot is shown in Fig. 4 whose slope gives the average particle size from the diffraction data and it is found to be 1.92 nm.

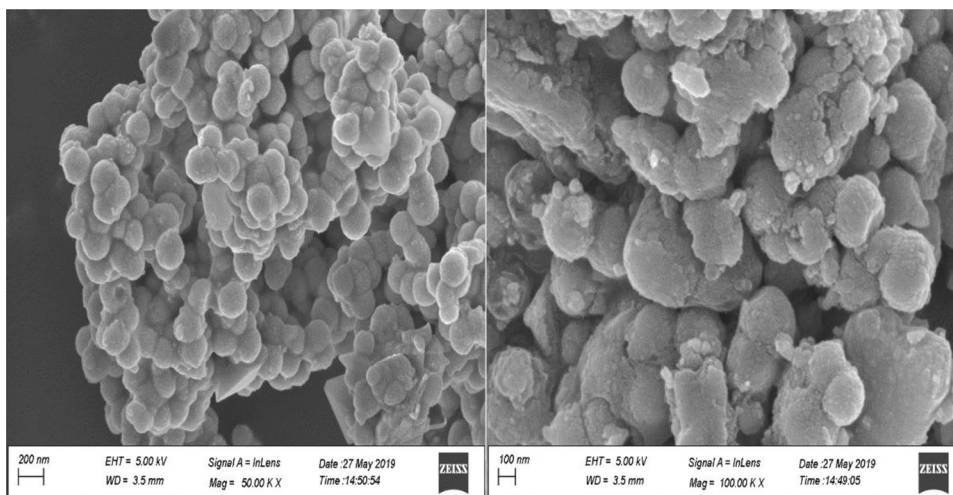
3.2 SEM analysis

The field emission scanning electron microscope (FESEM) images are showing the distribution of particles within the sample and the surface morphology of the particles as shown in Fig. 5. The spherical shaped nanoparticles are distributed uniformly over the sample and the surfaces of the particles are smooth. To investigate the elemental composition the energy dispersive spectroscopy (EDS) is used. The EDS spectra for as-synthesized CdSe is shown in Fig. 5. The presence of Cd and Se element with a very low amount of impurity is observed from the spectra. The weights of various elements forming CdSe nanostructures are shown in the inset table of Fig. 6.

3.3 TEM analysis

For more accurate structural observation on the nanoparticles high resolution TEM is used on the sample C.1 M. Four images of TEM is shown in Fig. 7. It is seen from Fig. 7 that the nanostructures are of almost spherical shape and well distributed over the solution. They also possess uniform size as seen from the images. The particle size is a bit larger than that of the Scherer plot of the XRD

Fig. 5 FESEM images of CdSe nanoparticles



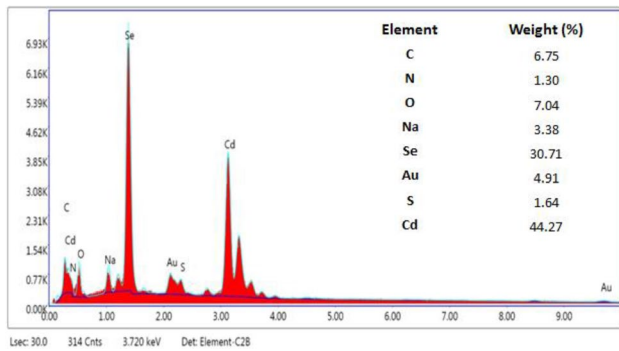
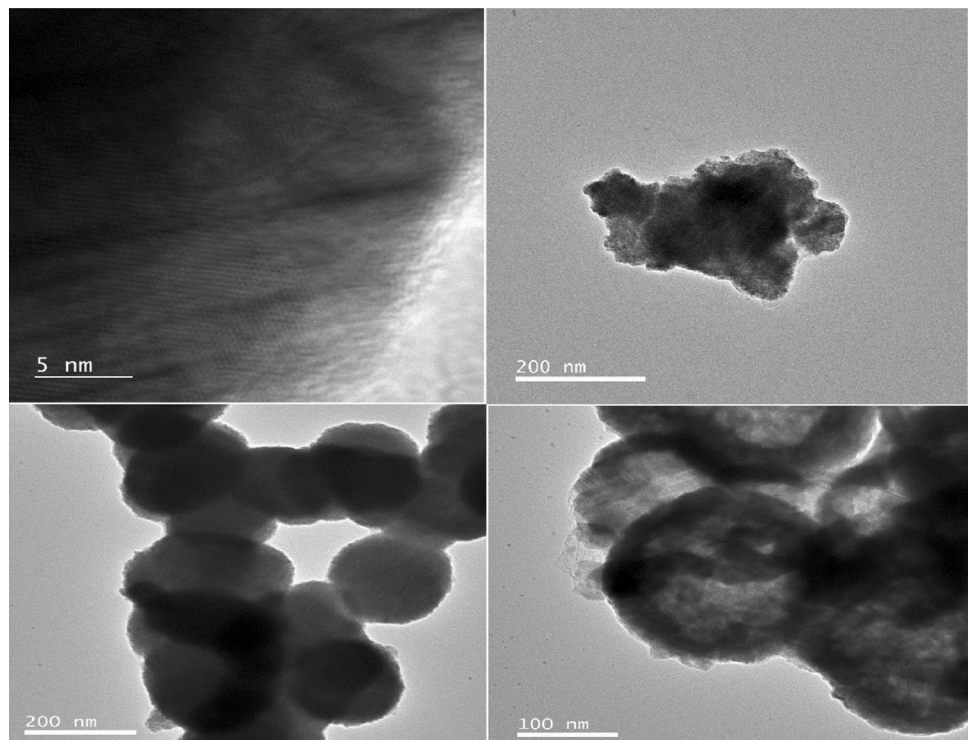


Fig. 6 EDS spectrum for CdSe nanoparticles and weights of various elements present in the sample (inset)

result and this the usual case. Moreover, Scherer equation assumes that the broadening of the diffraction peak of the XRD spectra can occur only due to the particle size. But in a real sense, the particle size can be influenced by some defects and other reasons due to which the particle size obtained from the TEM sometime varies slightly with the XRD result. The deviation of crystallite size calculated from XRD is several times smaller than the results found from TEM measurements. It may be attributed to the fact that in XRD measurements, the crystallite sizes are considered as sizes of “coherently diffracting domains” of crystals, whereas grains may contain several of these domains [27]. The cross lattice fringe signifies its superlattice nature of structure.

Fig. 7 HRTEM images of CdSe nanoparticles (C0.5 M)



3.4 FTIR analysis

The FTIR spectra contain the information on how the surface ligands and various functional groups of the chemicals and reagents are attached to stabilize the surface of the CdSe nanoparticles. Figure 8 represents the infrared spectra for CdSe nanoparticles stabilized by various groups and ligands. A broad and strong band appears at 3279.09 cm^{-1} due to the N–H vibration stretching of hydrazine hydrate. The sharp and intense band appears at 1602.12 cm^{-1} is due to the presence of O–H stretching vibration of the aqueous medium used as a solvent during the synthesis. Likewise, the bond at 1274 cm^{-1} is appearing due to the C–N stretching vibration of PVP used as the capping agent. The weak band at 1148 cm^{-1} is also due to the C–N stretching vibration as a result of the interaction of PVP and hydrazine hydrate. The band appearing at 623.22 cm^{-1} is responsible for the vibration of Cd–Se [28].

3.5 UV–Vis analysis

The UV–Vis absorption spectra are obtained for all the samples using a UV spectrometer as shown in Fig. 9. All the samples are showing a blue shift than the bulk counterpart of CdSe which is around 712 nm. This blue shift of absorption edges may be due to the quantum confinement which leads to the enhancement of band gaps in these samples. The Tauc’s relation for optical transition is given as in Eq. (3). The value of n is taken as 2 assuming the direct transition

Fig. 8 FTIR spectra for CdSe nanoparticles

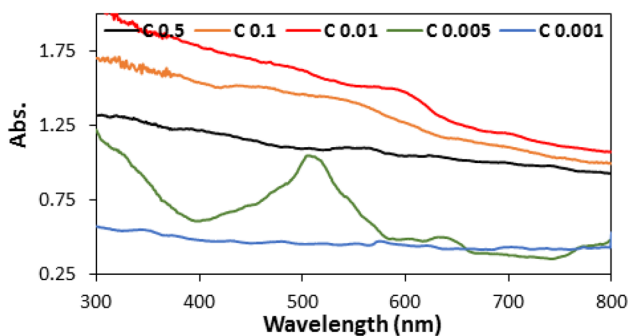
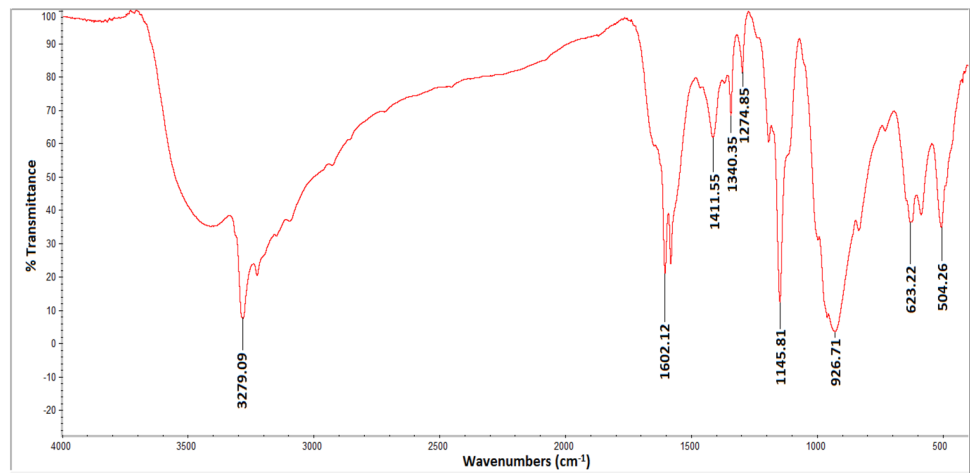


Fig. 9 Absorption spectra for various samples of CdSe nanoparticles

$$ahv = A(hv - E_g)^n \tag{3}$$

The Tauc's plots have been employed to estimate the band gaps of all samples as shown in Fig. 10. The band gaps are found as around 1.77 eV, 1.79 eV, 1.83 eV, 2.04 eV and 2.45 eV for C0.5 M, C0.1 M, C0.01 M, C0.005 M and C0.001 M respectively. It is observed from the values of band gaps that the bandgap of the samples are increasing with the decrease of the molar concentration of the samples as shown in Fig. 11. The Brus equation is a well-known and largely used method for determining the size of the

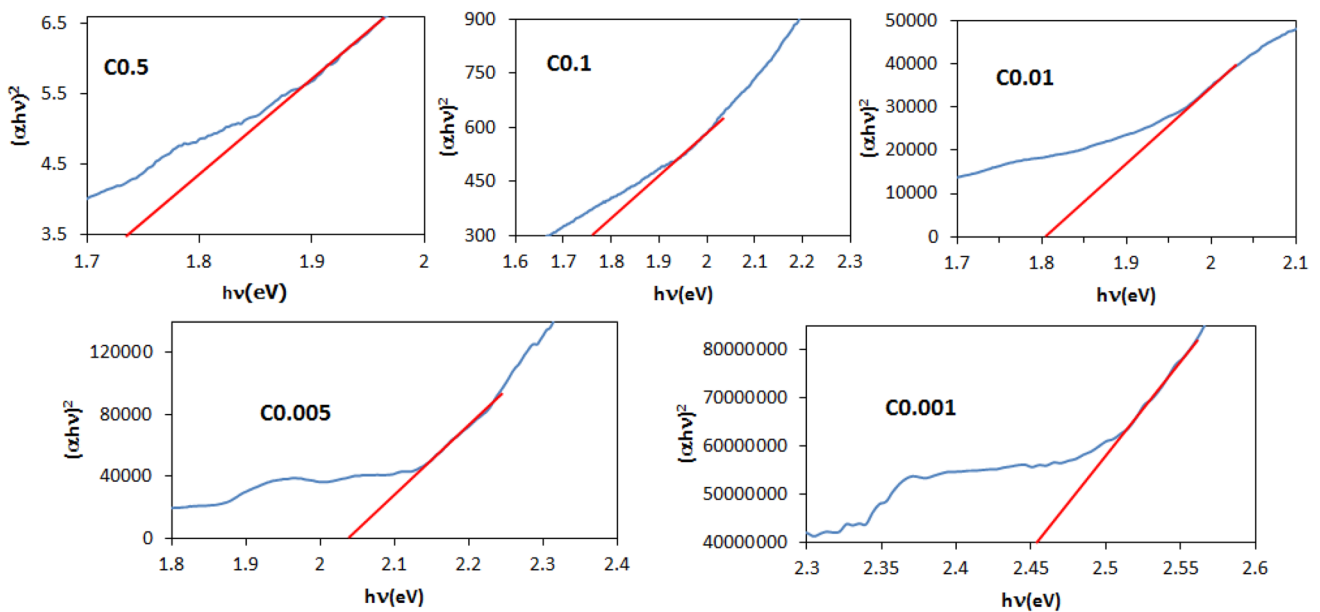


Fig. 10 Tauc's plot for CdSe nanoparticles synthesized with different Cd ion concentration

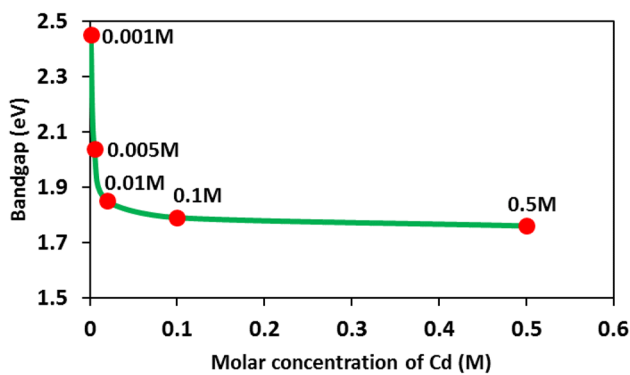


Fig. 11 Variation of band gap for CdSe nanoparticles with Cd ion concentration

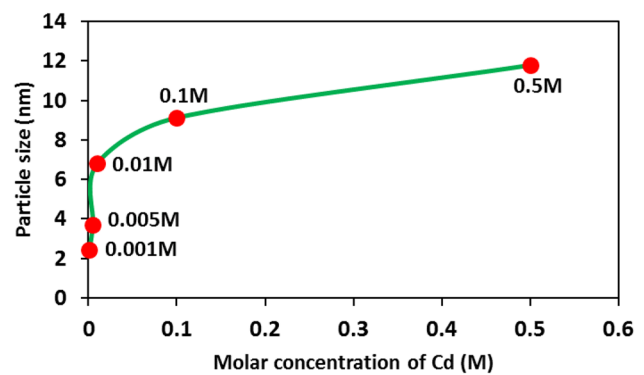


Fig. 12 Variation of particle size for CdSe nanoparticles with respect to Cd ion concentration

nanoparticles from the absorption data as shown in Eq. (4) where, m_e^* and m_h^* are the effective masses of the electron and hole for CdSe. The values of m_e^* and m_h^* are $0.13m_0$ and $0.3m_0$ respectively [29]. Where m_0 is the mass of the electron. E_g and E_g^{bulk} are the bandgaps of nanosized and bulk CdSe while ϵ is the dielectric permittivity of CdSe. This relation can be derived assuming the effective mass approximation method. The Brus equation has been used to calculate the size of the as-synthesized nanoparticles as in Eq. (4)

$$E_g = E_g^{\text{bulk}} + \frac{h^2}{8R^2} \left(\frac{1}{m_e^*} + \frac{1}{m_h^*} \right) - 1.8 \frac{e^2}{4\pi\epsilon R}. \quad (4)$$

The particle sizes obtained from the above relation are 11.78 nm, 9.12 nm, 6.81 nm, 3.72 nm, and 2.42 nm for C0.5 M, C0.1 M, C0.01 M, C0.005 and C0.001 M respectively. It is seen that the samples have a tendency to decrease the size of the particles with the decrease of molar concentration as shown in Fig. 12. This may be attributed to the slow rate of reaction among the constituent Cd and Se ion sources. As the concentration of Cd ion in the solution decreases the growth of CdSe nanoparticles in the reaction mixture will slow down. The functional groups of PVP will cap the smaller size particles preventing further growth on them which results in strong quantum confinement for the sample with lower Cd ion concentration. Various optical parameters such as bandgap and particle size pertaining to various samples of CdSe nanoparticles are presented in Table 1.

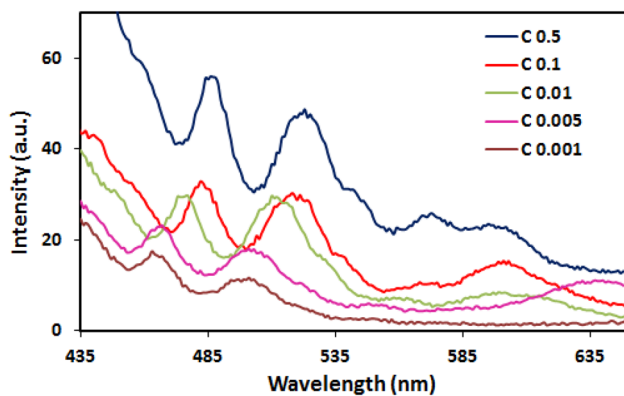
3.6 Photoluminescence analysis

The photoluminescence spectra of the prepared samples are shown in Fig. 13. The spectra are taken with the help of a fluorescence spectrometer with excitation wavelength 350 nm at continuous scanning mode from 435 to 650 nm.

The spectra of all the samples are showing the typical nature of CdSe nanostructures consisting of two peaks along with some energetically different mid gap impurity state emissions. Various defects that may be incorporated with the higher wavelength emissions are cation (or Cd^{2+}) vacancy, anion (or Se^{2-}) vacancy defects, oxygen at nanoparticle surface, and Se/Cd di-vacancy defect [30–32] as shown in Fig. 14a. The two sharp and distinct emissions in the visible region towards the low wavelength region around 460–530 nm can be assigned to the excitonic emissions in the nanocrystal [33]. The spectra clearly show a redshift of their emission edges with the increasing molar concentration of Cd ion complex. The full-width half maxima (FWHM) of the emission peaks are also getting decreased as we move from low to a high concentration of Cd ion in the samples. A large value of FWHM in PL peak indicates the non-uniform distribution of a large set of particles with different sizes. Therefore here we can conclude that the increase of cadmium ion concentration in the CdSe solution may lead to a uniform distribution of particles with less varying sizes. The fair distribution of particles with the uniform size is observed in the TEM images also. The PL intensities of the samples are also getting increased with the increase in concentration. The highest PL intensity of the sample C0.5 with concentration 0.5 M makes this material suitable for light-emitting devices. An enhanced PL intensity may be attributed to better crystallinity of the samples. Thus increasing the molar concentration in the range from 0.001 to 0.5 M the crystalline properties become feasible. In the wavelength range 545 to 635 nm, the sample C0.5 contains two broad emissions at around 575 nm and 600 nm. The emission at 575 nm is due to the Cd vacancies at the surface of CdSe nanocrystals. The broad emission peak at around 600 nm can be assigned to the charge recombination at the surface mid gap states due to the presence of an excessive amount of selenium present in the synthesized CdSe nanoparticles

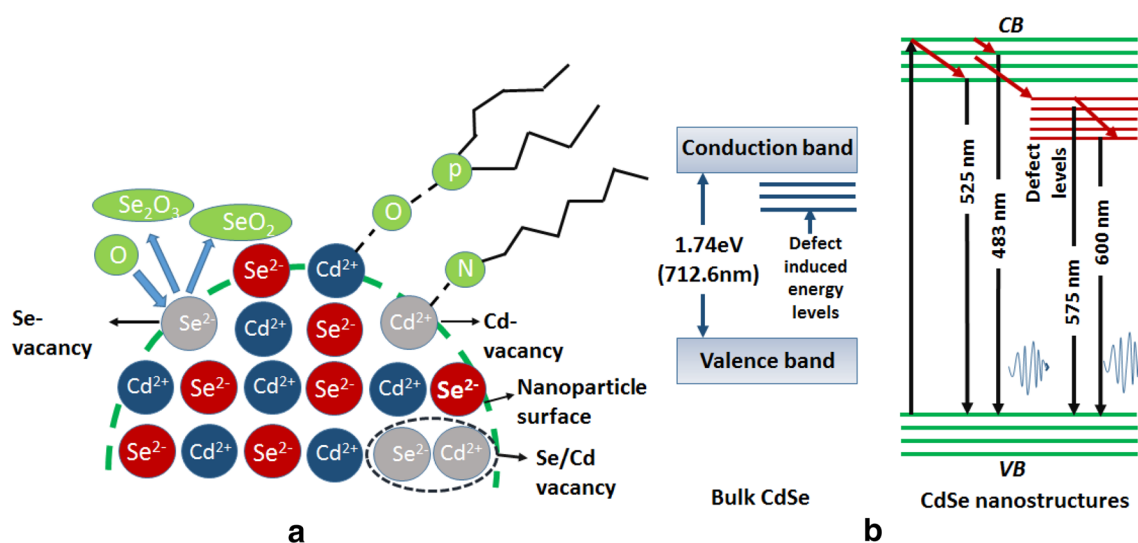
Table 1 Estimation of bandgap and particle size for CdSe nanoparticles

Sample	λ_{nbe} (nm)	PL intensity (a.u.)	Band-gap (eV) (from Tauc's plot)	Particle-size (nm)
C0.5	483	55.20	1.77	11.78
	525	47.59		
C0.1	479	36	1.79	9.12
	518	30.28		
C0.01	474	30.31	1.83	6.81
	511	29.13		
C0.005	470	22.12	2.04	3.72
	501	17.46		
C0.001	498	11.26	2.45	2.42

**Fig. 13** PL Spectra for CdSe nanoparticles with various molar concentration of Cd ions

[34, 35]. The energy states of bulk CdSe as well as various surface states of CdSe nanocrystal with its emissions are depicted in Fig. 14b. The presence of an excessive amount of selenium in the sample is also reflected at the

SEM-EDS spectra. This defect induced emission gradually become broad with the decrease of Cd ion concentration. For the sample prepared with concentration 0.001 M the tail of the PL spectra is getting flattened with no distinct peaks at the high wavelength region. In the case of sample C0.05 this peak is broadened and the emission covers all the wavelengths ranging from 572 to 602 nm. This may lead to a better application of this particular sample in the generation of white light in various optoelectronic devices. As the concentration of Cd ion decreases the intensity of the emission also decreases significantly. This may be due to the reason that at lower concentration the rate of the reaction between the Cd and Se ion will slow down, thus resulting a strong quantum confinement. The surface to volume ratio will become appreciably larger due to this quantum confinement and the carriers of the exciton pairs will be trapped at those created surface states. This leads to the elimination of various radiative recombination paths is also supported by the I-V characteristics curves of the samples which show that with the increase of quantum

**Fig. 14** Schematic diagram of the surface states for CdSe nanoparticle (a), Energy level diagram for bulk and nanosized CdSe (b)

confinement the photocurrent increases. Various optical parameters from absorption and PL data are represented in Table 1.

3.7 I–V characteristics

The room temperature I–V characteristics of the white light photosensor fabricated with five samples (C0.5, C0.1, C0.01, C0.005, C0.001) of CdSe nanoparticles as channel and Cu electrodes under the dark and illumination with white visible light are shown in Fig. 15. The symmetric and almost linear curves under dark condition and illumination with visible light suggest that the contact between the CdSe nanoparticle and Cu electrode is ohmic in nature. This may be attributed to surface defects and impurities [36]. As a result of the ohmic contact between the CdSe channel and Cu electrode, a good number of photoconductive paths are created which helps in the rapid transport of photoelectrons from CdSe film to Cu electrodes. In Fig. 15 the dark current curve is taken as common for all the devices as those are overlapped up to a bias voltage 5 V. For taking the I–V response curve under illumination the devices are illuminated with visible-light using a halogen lamp set up attached with Keithley source meter. As it is seen from the I–V response curve that the current across the channel increases significantly from 0.175 μA to 4.94 μA on illumination for the device fabricated with C0.5 sample of CdSe nanoparticles. For other devices also the photocurrent increases from 0.175 μA to 7.84 μA , 10.5 μA , 14.86 μA , and 16.16 μA for C0.1, C0.01, C0.005, and C0.001 respectively. In general, the increase of photocurrent under illumination with photon can be attributed to the fact that the increase of light absorption by the material leads to more number of electron–hole pair generation which will

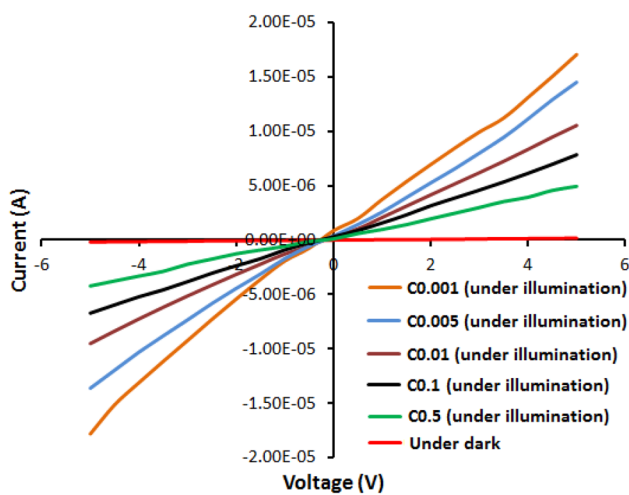


Fig. 15 I–V characteristics curve of a photosensor using CdSe sample of nanoparticles with various Cd ion concentration as channel and Cu as electrode under dark and illumination with visible light

contribute to the respective conduction and valence band and thereby increasing the photocurrent. Under illumination with a specific light of energy equal to or greater than the bandgap, a large number of exciton pairs are generated via optical absorption. These electron–hole pairs are recombined rapidly within the semiconductor. Some of those are separated at the Cu–CdSe metal–semiconductor junction by an external potential that produces the photocurrent. Under dark conditions, a large number of oxygen molecules from the air are absorbed by the semiconductor channel and those oxygen molecules again absorb the CdSe nanoparticles to form oxygen ions (O_2^-) by capturing electrons from n-type CdSe nanoparticles. As a result of this, a depletion layer is created which reduces the number of electrons at the metal–semiconductor interface, thus decreasing the dark current [37, 38]. As it is already mentioned that under illumination the number of photogenerated electron–hole pairs has been increased, that extra photo generated holes will occupy the surface states of CdSe nanoparticles. The O_2^- ions at the surface of CdSe nanoparticles will get discharged by absorbing those photogenerated holes. As a result of this more photogenerated electrons will get accumulated and reduce the radiative recombination thus significantly increasing the photocurrent [36, 38–40]. Another mechanism that supports the increase of photocurrent is the crystallinity of the nanoparticles. From the XRD spectra a good nanocrystallinity is realized for the as-synthesized CdSe nanoparticles. The high crystallinity possessed by the CdSe nanoparticles used as the channel in fabricating the device also reduces the recombination rate which increases the lifetime of the carriers in their respective bands and as a result the photocurrent increases [41]. Thus besides the band gap, a number of factors such as surface states, crystallinity etc. are expected to contribute to the significant enhancement of photocurrent.

A linear increase of photocurrent with the decrease of the molar concentration of Cd ion complex used as the channel can be observed from Fig. 15. This may be attributed to the quantum confinement in the samples of CdSe nanoparticles. From the absorption data it is seen that the bandgap increases with the decrease of the molar concentration of Cd ion complex. As the bandgap increases, the rate of radiative recombination decreases thus increasing the photoconduction. Moreover with the increase of quantum confinement the surface states of the nanoparticle increases which leads to the generation of a large number of surface trap states and reduce the recombination. As a result of this, the carriers of the photogenerated electron–hole pairs are separated and contribute to the photoconductivity. Thus the photocurrent increases with the increase of quantum confinement in the particles.

In order to assess the quality performance of a photodetector, photosensitivity (P_s), responsivity (R_λ), detectivity

(D^*) and external quantum efficiency (EQE) are some inevitable parameters [42, 43]. Photosensitivity of a photodetector is the measure upto which an object reacts on receiving photons and can be calculated as follows

$$P_s = (I_p - I_D)/I_D, \quad (5)$$

where P_s is the photosensitivity, I_p and I_D denotes the photocurrent and dark current respectively. The variation of photosensitivity with the molar concentration of Cd precursors is shown in Fig. 16a. It decreases with the increase of Cd concentration. Responsivity (R_λ) is another important parameter for photoelectric devices which can be defined as the measure of generated photocurrent for a particular sensing area per unit power of incident light and can be calculated with the following equation

$$R_\lambda = (I_p - I_D)/P_{\text{ill}}, \quad (6)$$

$$P_{\text{ill}} = I_{\text{ill}} \times A, \quad (7)$$

where, P_{ill} is the excitation power which again can be obtained by using Eq. (7), I_{ill} and A are the illumination density and effective device sensing area of the photodetector respectively. From Fig. 16b which shows the variation of responsivity with respect to molar concentration, it is seen that the responsivity increases linearly upto a concentration of 0.01 M and more sharply beyond this concentration. Detectivity (D^*) is the ability of the photodetector to detect the weakest signal of photon falling on the sensing area and can be obtained as follows.

$$D^* = R_\lambda \times (A)^{0.5} / (2 \times e \times I_D)^{0.5}. \quad (8)$$

The values of detectivity for different photodetectors are found in the range 111.85×10^9 Jones to 375.27×10^9 Jones. Besides these, external quantum efficiency (EQE) of a photodetector which is related to the number of generated exciton pairs can be calculated as follows

$$\text{ECE} = hc \times R_\lambda / \lambda. \quad (9)$$

The variation of detectivity and EQE are shown in Fig. 16c, d respectively. Both the figures show the same pattern that the detectivity and the EQE decrease with an increase in molar concentration of Cd ion complex. The values of these parameters for different Cd ion concentration based photodetectors are represented in Table 2.

It is worthwhile to mention that the above-obtained values of various parameters for CdSe nanoparticle-based photodetectors are quite satisfying compared to other relevant works. Prashad et al. [36] fabricated and studied the photoresponse characteristics of ZnS nanostructure-based UV-photodetectors and they have found responsivity in the range 1.2881 to 2.6158 $\mu\text{A}/\text{mW}$ and detectivity in the range 0.26×10^9 to 0.36×10^9 Jones. M. Patel et al. [44] fabricated highly efficient UV-photodetectors using p-NiO/n-ZnO heterojunction and obtained tremendously high responsivity and detectivity as 3.85 A/W and 9.6×10^{13} Jones respectively. Thus the values of parameters come out from our work is not significantly higher but lies within the range obtained by other workers in this field.

Fig. 16 Variation of photosensitivity (a), responsivity (b), detectivity (c) and EQE (d) with respect to Cd ion concentration for CdSe based photodetectors

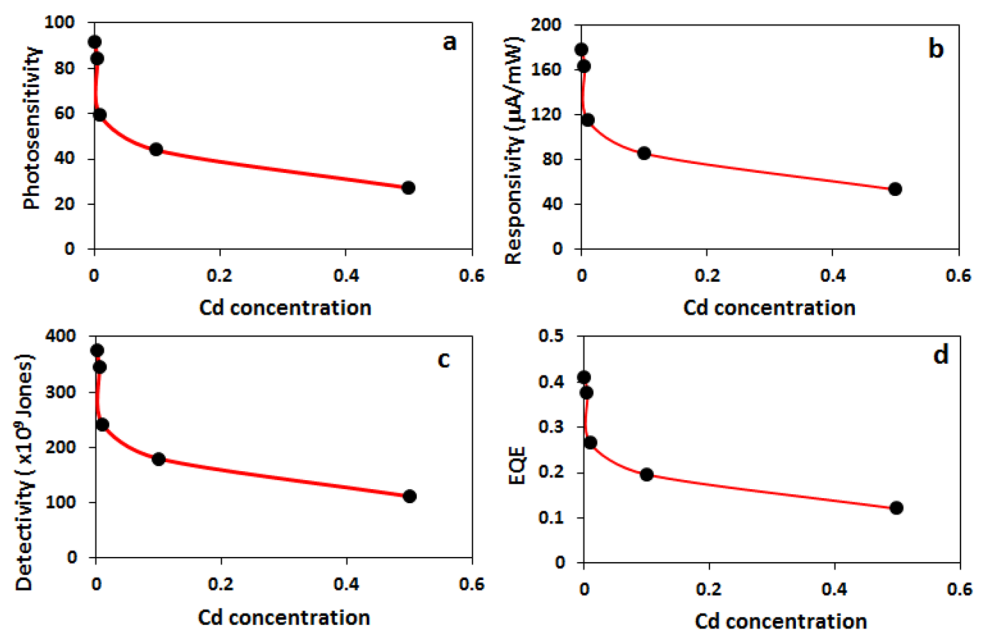


Table 2 Calculated parameters for CdSe nanoparticle-based photodetectors

Photodetector with Cd concentration	Dark current, I_D (mA)	Photocurrent, I_p (mA)	Photosensitivity	Responsivity, R_λ ($\mu\text{A}/\text{mW}$)	Detectivity, D^* ($\times 10^9$ Jones)	EQE
C0.5	0.175	4.94	27.22	52.94	111.85	0.12
C0.1	0.175	7.84	43.80	85.16	179.93	0.19
C0.01	0.175	10.5	59	114.72	242.39	0.26
C0.005	0.175	14.86	83.91	163.16	344.73	0.37
C0.001	0.175	16.16	91.34	177.61	375.27	0.40

4 Conclusion

In conclusion, this work has a meaningful exploration of the effects of Cd ion concentration towards the reaction dynamics in the formation of CdSe nanoparticles through the cost-effective chemical bath deposition technique at room temperature. It is found that a low concentration of Cd ion complex leads to better quantum confinement on CdSe nanoparticles and better efficiency in the fabricated white light photosensors with synthesized CdSe nanoparticles as the channel in the devices. From the absorption data, it is seen that decrease of Cd ion concentration leads to strong quantum confinement on the CdSe nanoparticles as well as enhancement of bandgap. Photoluminescence spectra show near bandgap emissions around 460–530 nm along with other impurity emissions. PL peaks are red-shifted along with an enhancement of intensity with the increase of Cd ion concentration. The impurity emission at 575 nm is due to the Cd vacancies at the surface of CdSe nanocrystals while emission around 600 nm can be assigned to the charge recombination at the surface mid gap states due to excess amount of selenium present in CdSe nanoparticles. This enhancement in the bandgap of the particles increases the photocurrent as well as the sensitivity of the photo-detector which is clearly reflected by their I–V characteristics. The I–V characteristics of the devices exhibit an ohmic nature. The photo-detector fabricated with CdSe nanoparticles synthesized with low Cd ion concentration shows a better response towards the white light. The photodetector characteristics parameters viz; photosensitivity, responsivity, detectivity, and EQE are found to be suitable maximum at lower Cd ion concentration. These sets of information may be quite useful in the fabrication of white light photosensor using PVP capped CdSe nanoparticles.

Acknowledgements Authors sincerely thank the Department of chemistry, Department of Physics Rajiv Gandhi University and Saif, Gauhati University for providing the necessary experimental facilities.

References

- H. Luo, B.A. Kebede, E.J. McLaurin, V. Chikan, Rapid induction and microwave heat-up syntheses of CdSe quantum dots. *ACS Omega* **3**(5), 5399–5405 (2018)
- P.K. Sahu, R. Das, R. Lalwani, Incorporation of tin in nanocrystalline CdSe thin films: a detailed study of optoelectronic and microstructural properties. *Appl. Phys. A Mater. Sci. Process.* **24**(665), 01–13 (2018)
- S. Yadav, A. Singh, L. Thulasidharan, S. Sapra, Surface decides the photoluminescence of colloidal CdSe nanoplatelets based core/shell heterostructures. *J. Phys. Chem. C* **122**(1), 820–829 (2018)
- V. Babentsov, F. Sizov, Defects in quantum dots of II–VI semiconductors. *Opto-electron Rev.* **16**, 208–225 (2006)
- N. Ordenes-Aenishanslins et al., Biological synthesis of CdS/CdSe core/shell nanoparticles and its application in quantum dot sensitize solar cells, 10, 1587 (2019) 1–10
- S. Sadeghi, S.K. Abkenar, C.W. Ow-Yang, S. Nizamoglu, Efficient white LEDs using liquid-State Magic sized CdSe Quantum Dots. *Sci. Rep* **9**, 1–9 (2019)
- C. Li, F. Wang, Y. Chen, L. Wu, X. He, B. Li, L. Feng, Characterization of sputtered CdSe thin films as the window layer for CdTe solar cells. *Mater. Sci. Semicond. Process* **83**, 89–95 (2018)
- D. Zhu, H. Ye, H. Zhen, X. Liu, Improved performance in green light-emitting diodes made with CdSe conjugated polymer composite. *Synth. Met.* **158**, 879–882 (2008)
- Y.P. Wei, X.P. Liu, C.J. Mao, H.L. Niu, J.M. Song, B.K. Jin, Highly sensitive electrochemical biosensor for streptavidin detection based on CdSe quantum dots. *Biosens. Bioelectron.* **103**, 99–103 (2018)
- R.B. Kale, C.D. Lokhande, Band gap shift, structural characterization and phase transformation of CdSe thin films from nanocrystalline cubic to nanorod hexagonal on air annealing. *Semicond. Sci. Technol.* **20**, 1–9 (2004)
- Q. Shen, D. Arae, T. Toyoda, Photosensitization of nanostructured TiO₂ with CdSe quantum dots: effects of microstructure and electron transport in TiO₂ substrates. *J. Photochem. Photobiol. A* **164**, 75–80 (2004)
- X. Zheng, Y. Xie, L. Zhu, X. Jiang, A. Yan, Formation of vesicle-templated CdSe hollow spheres in an ultrasound-induced anionic surfactant solution. *Ultrasonics Sonochem.* **9**, 311–316 (2002)
- O. Palchik, R. Kerner, A. Gedanken, A.M. Weiss, M.A. Slifkin, V. Palchik, Microwave-assisted polyol method for the preparation of CdSe nanoballs. *J. Mater. Chem* **11**, 874–878 (2001)
- M. Sharma, S. Kumar, O.P. Pandey, Photo-physical and morphological studies of organically passivated core–shell ZnS nanoparticles. *Dig. J. Nanomater. Bios.* **3**(4), 189–197 (2008)
- W. Jin, L. Hu, Review on quasi one-dimensional cdse nanomaterials: synthesis and application in photodetectors. *Nanomaterials* **9**, 1–19 (2019)
- H. Yu, J. Li, R.A. Loomis, P.C. Gibbons, L.W. Wang, W.E. Buhro, Cadmium selenide quantum wires and the transition from 3D to 2D confinement. *J. Am. Chem. Soc.* **125**, 16168–16169 (2003)
- Z. Gao, W. Jin, Y. Zhou, Y. Dai, B. Yu, C. Liu, W. Xu, Y. Li, H. Peng, Z. Liu et al., Self- powered flexible and transparent

- photovoltaic detectors based on CdSe nanobelt/graphene Schottky junctions. *Nanoscale* **5**, 5576–5581 (2013)
18. W. Jin, K. Zhang, Z. Gao, Y. Li, L. Yao, Y. Wang, L. Dai, CdSe nanowire-based flexible devices: Schottky diodes, metal–semiconductor field-effect transistors, and inverters. *ACS Appl. Mater. Interfaces* **7**, 13131–13136 (2015)
 19. T. Zhai, L. Li, X. Wang, X. Fang, Y. Bando, D. Golberg, Recent developments in one-dimensional inorganic nanostructures for photodetectors. *Adv. Funct. Mater* **20**, 4233–4248 (2010)
 20. K. Senthilkumar, T. Kalaivani, S. Kanagesan, V. Balasubramanian, Synthesis and characterization studies of ZnSe quantum dots. *J. Mater. Sci. Mater. Electron.* **23**, 2048–2052 (2012)
 21. P. Li, B. Zhu, P. Li, Z. Zhang, L. Li, Y. Gu, A facile method to synthesize CdSe-reduced graphene oxide composite with good dispersion and high Nonlinear optical properties. *Nanomaterials* **9**(957), 1–13 (2019)
 22. R. Divya, N. Manikandan, T.C. Sabari Girisun, G. Vinitha, Investigations on the structural, morphological, linear and third order nonlinear optical properties of manganese doped zinc selenide nanoparticles for optical limiting application. *Opt. Mater* **100**(109641), 1–13 (2020)
 23. L. Saravanan, S. Diwakar, R. Mohankumar, A. Pandurangan, R. Jayavel, Synthesis, structural and optical properties of PVP encapsulated CdS nanoparticles. *Nanomater. Nanotechnol.* **1**(2), 42–48 (2011)
 24. K.F. Chepape, T.P. Mofokeng, P. Nyamukamba, K.P. Mubiayi, M.J. Moloto, Enhancing photocatalytic degradation of methyl blue using PVP-capped and uncapped CdSe nanoparticles. *J. Nanotechnol.* **5340784**, 1–6 (2017)
 25. M. Safo, C.D. Werheid, M. Oezaslan, The role of polyvinylpyrrolidone (PVP) as a capping and structure-directing agent in the formation of Pt nanocubes. *Nanoscale Adv.* **1**, 3095–3106 (2019)
 26. N.B. Brahim, N.B.H. Mohamed, M. Echabaane, M. Haouari, R.B. Chabaane, M. Nigrierie, H.B. Quada, Thioglycerol -functionalized CdSe quantum dots detecting cadmium ions. *Sens. Actuators B Chem* **220**, 1346–1353 (2015)
 27. J. Henry, T. Daniel, V. Balasubramanian, K. Mohanraj, G. Sivakumar, Enhanced photosensitivity of bi-doped Cu₂Se thin films prepared by chemical synthesis for solar cell application. *Iran J Sci Technol Trans Sci*, 2020, 1–9
 28. Muthukannan, G. Sivakumar, and K. Mohanraj, Influence of Equimolar Concentration on Structural and Optical Properties of Binary Selenides Nanoparticles, *Particulate Science and Technology*, **32** (2014) 392–398
 29. A. Mukherjee and S. Ghosh, Optimum excitation photon energy for CdSe–ZnS core–shell quantumdot based luminescence imaging, *J. Phys. D: Appl. Phys.* **45**, 195103 (2012) 1–5
 30. S. Mathew, V.R. Anand, A.A. Correya, V.P.N. Nampoore, A. Mujeeb, Surface defect assisted broad spectra emission from CdSe quantum dots for white LED application. *Mater. Res. Express* **5**, 025009 (2018)
 31. E. Kucur, W. Bücking, T. Nann, Electrochemical determination of mesoscopic phenomena, defect states in CdSe nanocrystals and charge carrier manipulability. *Microchim Acta* **160**, 299–308 (2008)
 32. E. Kucur, W. Bücking, R. Giernoth, T. Nann, Determination of defect states in semiconductor nanocrystals by cyclic voltammetry. *J. Phys. Chem. B* **109**(43), 20355–20360 (2005)
 33. S. Mathew, S.A. Joseph, P. Radhakrishnan, V.P.N. Nampoore, C.P.G. Vallabhan, Shifting of fluorescence peak in CdS nanoparticles by excitation wavelength change. *J Fluoresc* **21**, 1479–1484 (2011)
 34. M.J. Bowers, J.R. McBride, S.J. Rosenthal, White-light emission from magic-sized cadmium selenide nanocrystals. *J. Am. Chem. Soc.* **127**, 15378–15379 (2005)
 35. N.A. Hill, K.B. Whaley, A theoretical study of the influence of the surface on the electronic structure of CdSe nanoclusters. *J. Chem. Phys.* **100**(4), 2831–2837 (1994)
 36. N. Prasad, B. Karthikeyan, Phase-dependent structural, optical, phonon and UV sensing properties of ZnS nanoparticles. *Nanotechnology* **30**, 485702–485716 (2019)
 37. P.T. Gomathi, P. Sahatiya, S. Badhulika, Large-area, flexible broadband photodetector based on ZnS–MoS₂ hybrid on paper substrate. *Adv. Funct. Mater.* **1701611**, 1–9 (2017)
 38. L. Hu, J. Yan, M. Liao, H. Xiang, X. Gong, L. Zhang, X. Fang, An optimized ultraviolet-A light photodetector with wide-range photoresponse based on ZnS/ZnO biaxial nanobelt. *Adv. Mater.* **24**, 2305–2309 (2012)
 39. J.S. Jie, W.J. Zhang, Y. Jiang, X.M. Meng, Y.Q. Li, S.T. Lee, Photoconductive characteristics of single-crystal CdS nanoribbons. *Nano Lett.* **6**, 1887–1892 (2006)
 40. M. Hajimazdarani, N. Naderi, B. Yarmand, Effect of temperature-dependent phase transformation on UV detection properties of zinc sulfide nanocrystals. *Mater. Res. Express* **6**(085096), 1–9 (2019)
 41. W. Zhao, L. Liu, M. Xu, X. Wang, T. Zhang, Y. Wang, Z. Zhang, S. Qin, Z. Liu, Single CdS nanorod for high responsivity UV–Visible photodetector. *Adv. Opt. Mater.* **1700159**, 1–7 (2017)
 42. X. Li, M. Zhu, M. Du, Z. Lv, L. Zhang, Y. Li, Y. Yang, T. Yang, X. Li, K. Wang, H. Zhu, Y. Fang, High detectivity graphene-silicon heterojunction photodetector. *Small* **12**(5), 595–601 (2016)
 43. Q. Hong, Y. Cao, J. Xu, H. Lu, J. He, J.L. Sun, Self-powered ultrafast broadband photodetector based on p-n heterojunctions of CuO/Si Nanowire Array. *ACS Appl. Mater. Interfaces* **6**, 20887–20894 (2014)
 44. M. Patel, H.S. Kim, J. Kim, All transparent metal oxide ultraviolet photodetector. *Adv. Electron. Mater* **1500232**(1), 1–9 (2015)

Publisher's Note Springer Nature remains neutral with regard to jurisdictional claims in published maps and institutional affiliations.